Copyright © 2009 Tech Science Press FDMP, vol.5, no.4, pp.313-330, 2009

Numerical Simulation of Three Dimensional Low Prandtl Liquid Flow in a Parallelepiped Cavity Under an external Magnetic Field

F. Mechighel[1,2], M. El Ganaoui[1], M. Kadja[2], B. Pateyron[3] and S. Dost[4]

Abstract: A numerical study has been carried out to investigate the three-dimensional buoyant flow in a parallelepiped box heated from below and partially from the two sidewalls (a configuration commonly used for solidification problems and crystal growth systems). Attention has been paid, in particular, to phenomena of symmetry breaking and transition to unsteady non-symmetric convection for a low Prandtl number fluid (Pr=0.01). The influence of an applied horizontal magnetic field on the stability properties of the flow has been also considered. Results obtained may be summarized as follows: In the absence of magnetic field and for relatively small values of the Rayleigh number (Ra), a steady and symmetric flow field is obtained with 3D effects limited to classical spiral flows in the third direction. When Ra is increased to its first critical value, the system bifurcates from the steady symmetric flow to a non-symmetric flow. The break in symmetry occurs with respect to the vertical mid-plane and the diagonal plane. The first critical value for which symmetry is broken has been found to behave as an increasing function of the magnetic field strength.

Keywords: Buoyant flow, break in symmetry, magnetic field.

1 Introduction

In most solidification and crystal growth processes such as the Bridgman, float-zone, travelling heater method, etc., the growth interface advances in the direction parallel to the gravity vector. Thus the density gradient in the melt/solution is parallel to gravity, and convection ensues when buoyancy overcomes viscous effects.

[1] University of Limoges, SPCTS UMR CNRS 6638, 123 avenue Albert Thomas, 87060 Limoges, France
[2] University of Constantine, 25000 Constantine, Algeria
[3] University of Limoges, SPCTS UMR CNRS 6638, 123 avenue Albert Thomas, 87060 Limoges, France
[4] Crystal Growth Laboratory, University of Victoria, Victoria, BC ,Canada V8W3P6

The onset of convective instability, as in the case of Rayleigh-Bénard convection, is characterized by the Rayleigh number. Fluids heated (from below and/or from the side) exhibit a very complex, non-linear behaviour. At critical values of the control parameters, the melt convective flow frequently becomes unstable and bifurcates from a stationary to steady or unsteady states. Critical values of this kind are called bifurcations. Bifurcation is a structural change in the flow at critical values of the control parameters and it plays an important role in the development of deterministic chaos. Furthermore, bifurcation instabilities in melt flows lead to the appearance of three-dimensional oscillatory effects (temperature oscillations) and non-symmetric flow structures which in turn lead to inhomogeneities in the structure of the growing crystals, affecting the crystal quality, see Müller and Ostrogorsky (1994).

The problem of bifurcation in convective flows was pointed out in the experimental works of Hurle (1966), and was shown that oscillations of convective flow cause striations in crystals growing from melts. Thus, the problem of onset of oscillatory instability of steady convective flows attracted great scientific interest, and has been studied extensively. For instance, Impey, Riley, Wheeler and Winters (1991) used the techniques of bifurcation theory to analyze the possible forms of steady, 2-D flow induced by solutal buoyancy forces in a dilute binary mixture during its vertical directional solidification. They focused on the role of lateral confinement in determining the flow patterns that are realizable in the melt. Gelfgat, Bar-Yoseph and Yarin (1999a) performed a parametric study of multiple steady states, their stability, onset of oscillatory instability, and some supercritical unsteady regimes of convective flow of a fluid with Pr=0.015 in laterally heated rectangular cavities. Also a study of the bifurcation of central symmetry breaking and stability of non-symmetric states of convection in laterally heated cavities was also carried out by Gelfgat, Bar-Yoseph and Yarin (1999b). Two and three-dimensional computations for different modes of Rayleigh-Bénard instability were performed by Gelfgat (1999). In addition, the critical stability limit for the onset of the natural convection in 2-D flows was investigated, and the threshold value for breaking symmetry and unsteadiness were identified by El Ganaoui and Bontoux (1998).

A recent work of Bennacer, El Ganaoui and Leonardi (2006) presented three-dimensional computations for an inverted Bridgman configuration and the fluid flow instability and transition to unsteadiness were analyzed. It was shown that the bifurcation type might change when a controlling parameter (Rayleigh number) was varied. Sheu, Rani, Tan and Tsai (2007) considered the same configuration and extended it to analyze the multiple states, topology and bifurcations of melt flow.

Other relevant and recent studies are due to Sahu, Muralidhar and Panigrahi (2007),

Prud'homme and El Ganaoui (2007), Achoubir, Bennacer, Cheddadi, El Ganaoui and Semma (2008), Bucchignani (2009).

The present study analyses numerically the three-dimensional character of low Prandtl number flows and focuses on the symmetry breaking phenomena which can produce some unsteadiness in the flow and consequently perturb the solid/liquid interface shape and dopant distribution.

In addition, the present work considers the possibility of stabilizing convective flow by means of an applied horizontal magnetic field. The literature on the use of magnetic fields in solidification, crystal growth, and flows (both experimental and theoretical) is very rich. These studies have addressed various issues involving the application of magnetic fields flow stability, flow suppression, interface stability, and growth rates. For instance, the effect of applied magnetic fields on flow structures, growth interface shapes, and growth rates in solution/melt crystal growth techniques can be found in works by: Kakimoto and Liu (2006), Dost and Lent (2007), Dost and Okano (2007), Liu, Dost, Lent and Redden (2003), Sheibani, Dost, Sakai, and Lent (2003), Liu, Dost and Sheibani (2004), Sohail and Saghir (2006), Kumar, Dost, Durst (2007), Yildiz, Dost (2007), and Armour, Yildiz, Yildiz and Dost (2008), and flow instability and electromagnetic damping in various flows in works by: Hurle, Jakeman and Johnson (1974), Hof, Juel and Mullin (2003), Okada and Ozoe (1992), Piazza and Ciofalo (2002), Gelfgat, Bar-Yoseph and Solan (2001), Dennis and Dulikravich (2002), and Touihri, Ben Hadid and Henry (1999). The electromagnetic damping of convective flows was experimentally and numerically studied for flows in 2-D rectangular cavities (such as in Hurle, Jakeman and Johnson (1974), Hof, Juel and Mullin (2003)), and in 3-D configurations (as in Okada and Ozoe (1992), Piazza and Ciofalo (2002)).

The effect of the magnetic field on the 3-D symmetry-breaking bifurcation of initially symmetric steady convective flows was recently studied in Gelfgat, Bar-Yoseph and Solan (2001), Dennis and Dulikravich (2002), and Touihri, Ben Hadid and Henry (1999). The geometry considered in these studies was cylindrical, and the temperature boundary conditions considered corresponds to the Rayleigh-Bénard problem.

Electromagnetic stabilization of symmetric convective flows in rectangular geometries with more complicated thermal conditions, however, such as in the present study, has not been widely studied. This was the motivation in carrying out the present study.

2 Mathematical formulation and numerical simulation of the problem

We consider the parallelepiped box (cavity) shown in Fig.1, which is filled with an electrically conducting low Prandtl number liquid metal (Pr = 0.01). The height of the cavity is denoted by Lx and is taken as the length scale of the problem. The length and the width of the cavity are Lz and Ly respectively (with: Lx = Ly = Lz = 100 mm).

The fluid in the cavity is heated from below (bottom) and cooled from top. The left and right walls are heated up to a dimensionless height H ($H = h_h/L_x = 0.75$) and are adiabatic in the remaining part (1 - H). The front and the rear walls are set to be adiabatic. The heated walls are maintained at a temperature (T_h), which corresponds to the temperature of the furnace in a crystal growth system. The top cooled wall is maintained at a lower temperature (T_c), which corresponds to the temperature at the solidification front. No heat flux is imposed. Thermo-physical properties (the thermal conductivity k, the dynamic viscosity μ and the thermal diffusivity α) of the fluid are taken as constants. The flow is assumed to be Newtonian, laminar, and incompressible with no viscous dissipation, and the Boussinesq approximations holds.

2.1 The Governing Equations

$\Omega \subset R^{n_{sd}}$ represents the spatial domain (Fig.1) at the time $t \in (0,\ t_{\max})$, where n_{sd} is the number of space dimensions, Γ is the boundary of Ω. The part of the boundary at which the temperature is prescribed (essential condition) is denoted by Γ_g. The Neumann (natural) boundary conditions are assumed to be imposed at the remaining part of the boundary Γ_h.

The following dimensionless scales and variables are adopted (respectively for coordinates, velocity components, pressure, time, temperature and electrical potential): $X = x/L_x$, $Y = y/L_x$; $Z = z/L_x$; $U = uL_x/\alpha$; $V = vL_x/\alpha$; $W = wL_x/\alpha$; $P = pL_x^2/\rho_l\alpha^2$; $\tau = t\,\alpha/L_x^2$; $\theta = (T - T_c)/\Delta T$ and $\Phi = \phi/\alpha B_0$ where:, ρ_l is the fluid density, (u, v, w) are the velocity components, B_0 the constant magnitude of the applied magnetic field and $\Delta T = T_h - T_c$ is the characteristic temperature difference.

With the above assumptions and using the dimensionless variables above, the dimensionless forms of the governing equations representing (mass, three-dimensional Navier-Stokes, energy and electrical potential equations) in τ_{stab} can be written, respectively, as:

$$\nabla \cdot \mathbf{U} = 0 \tag{1}$$

$$\partial \mathbf{U}/\partial \tau + (\mathbf{U}\cdot\nabla)\mathbf{U} = -\nabla P + \mathrm{Pr}\nabla^2\mathbf{U} - \mathrm{Pr}\,Ra\,\theta\,\mathbf{e_g} + \mathrm{Pr}\,Ha^2\left[-\nabla\Phi + \mathbf{U}\times\mathbf{e_B}\right]\times\mathbf{e_B}$$

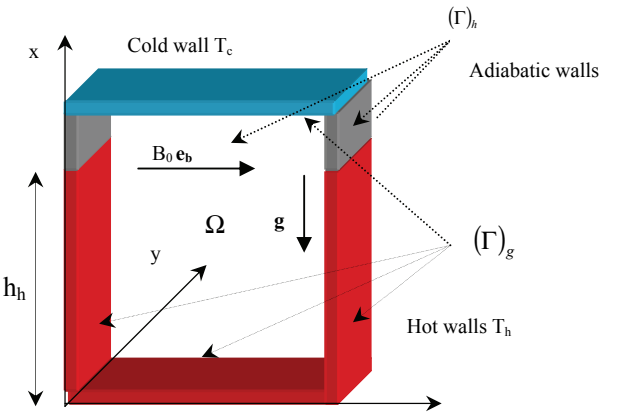

Figure 1: The model domain geometry and boundary conditions

which can expressed as:

$$\partial \mathbf{U}/\partial \tau + (\mathbf{U}\cdot\nabla)\mathbf{U} - \nabla\boldsymbol{\sigma} = -\Pr Ra\,\theta\,\mathbf{e_g} + \Pr Ha^2\left[-\nabla\Phi + \mathbf{U}\times\mathbf{e_B}\right]\times\mathbf{e_B} \tag{2}$$

where: $\boldsymbol{\sigma}(P,\mathbf{U}) = -P\mathbf{I} + 2\Pr\boldsymbol{\varepsilon}(\mathbf{U})$; and with: $\boldsymbol{\varepsilon}(\mathbf{U}) = \frac{1}{2}\left[\nabla\mathbf{U} + (\nabla\mathbf{U})^T\right]$,

$$\partial\theta/\partial\tau + (\mathbf{U}\cdot\nabla)\,\theta = \nabla^2\theta \tag{3}$$

$$\nabla^2\Phi = \nabla\cdot(\mathbf{U}\times\mathbf{B}) = Ha^2\Pr\mathbf{e_B}\cdot(\nabla\times\mathbf{U}) \tag{4}$$

where $\mathbf{U}(\mathbf{X},\,\tau)$ is the dimensionless vector velocity, $\Pr = \nu/\alpha$ the Prandtl number, ν kinematic viscosity, $Ra = g\beta_T\Delta T L_x/\nu\alpha$ the thermal Rayleigh number, g the gravity acceleration, β_T the coefficient of thermal expansion, $Ha = B_0 L_x\sqrt{\sigma_e/\nu\rho_l}$ the Hartmann number, σ_e the electrical conductivity of the liquid,$\mathbf{e_g}$ is the unit vector in the direction of the gravity and $\mathbf{e_B}$ is the vector unit in the direction of the magnetic field.

We assume no-slip boundary condition for that the flow velocity on the entire boundaries of the domain

$$\mathbf{U}(\mathbf{X},\tau) = \mathbf{0} \text{ on } \Gamma\,\forall\tau\in(0,\ \tau_{\max}) \tag{5}$$

The dimensionless temperature boundary conditions are:

$$\theta(0,Y,Z,\tau) = 1, \quad \theta(1,Y,Z,\tau) = 0, \quad \theta(X,Y,0,\tau) = \theta(X,Y,1,\tau) = 1$$

for $0 < X < H$,

$(\partial\theta/\partial Z)_{(X,Y,0,\tau)} = (\partial\theta/\partial Z)_{(X,Y,1,\tau)} = 0$

for $H < X < 1$, and

$(\partial\theta/\partial Y)_{(X,0,Z,\tau)} = (\partial\theta/\partial Y)_{(X,1,Z,\tau)} = 0$

The dimensionless electric potential function conditions on the boundary

$\nabla\Phi(\mathbf{X},t)\cdot\mathbf{n} = 0$ on $\Gamma\times(0,\tau_{\max})$

Initial conditions on Ω_0 are taken as

$$\mathbf{U}(\mathbf{X},0) = 0, \quad T(\mathbf{X},0) = 0 \text{ and } \Phi(\mathbf{X},0) = 0 \tag{6}$$

2.2 Finite element Formulations

2.2.1 A stabilized Galerkin/Least Square FEM for Unsteady Incompressible Flow

Standard Galerkin finite element analysis of incompressible flows can introduce two main sources of potential numerical instabilities. The first one is due to the presence of advection terms in the governing equations, and can result in spurious oscillations in the velocity field. The second is due to using inappropriate combinations of interpolation functions to represent the velocity and pressure fields. The Stabilized Galerkin/Least-Square (GLS) finite element formulation is used here in order to prevent such numerical instabilities (details on this technique can be found in works by Tezduyar, Mittal, Ray and Shih (1992) and Tezduyar (1992)).

In the present work, this method was extended for the simulation of incompressible fluid flows to handle the 3-D flow driven by the combination of buoyancy and electromagnetic body forces. This stabilized finite element formulation was utilized using equal-order interpolation velocity-pressure elements as proposed by Tezduyar, Mittal, Ray and Shih (1992) and Tezduyar (1992).

2.2.2 The Space-Time Formulation and GLS Stabilization

In the space-time finite element formulation, the time interval $(0, t_{max})$ is partitioned into subintervals $I_n = (t_n,\ t_{n+1})$, where $t_n$and t_{n+1} belong to an ordered series of time levels $0 = t_0 < t_1 < \cdots < t_N = t_{\max}$. The space-time slab Q_n is defined as the space-time domain $\Omega\times I_n$. The lateral surface of Q_n is denoted by P_n; this is the surface described by the boundary Γ, as t traverses I_n.

Finite element discretization of a space-time slab Q_n is achieved by dividing it into elements Q_n^e, $e = 1, 2, \cdots, (n_{el})_n$, where $(n_{el})_n$ is the number of elements in the

space-time slab Q_n. Associated with this discretization, for each space-time slab we define the following finite element interpolation function spaces for the velocity and pressure

$$\left(S_{\mathbf{u}}^h\right)_n = \left\{ \mathbf{u}^h \,\middle|\, \mathbf{u}^h \in \left[H_0^{1h}(Q_n)\right]^{n_{sd}},\ \mathbf{u}^h = 0 \text{ on } P_n \right\}$$

$$\left(V_{\mathbf{u}}^h\right)_n = \left\{ \mathbf{w}^h \,\middle|\, \mathbf{w}^h \in \left[H_0^{1h}(Q_n)\right]^{n_{sd}},\ \mathbf{w}^h = 0 \text{ on } P_n \right\}$$

$$\left(S_p^h\right)_n = \left(V_p^h\right)_n = \left\{ q^h \,|\, q^h \in H_0^{1h}(Q_n) \right\}$$

where $\mathbf{w}^h$ represents the weighting functions and $H_0^{1h}(Q_n)$ the finite-dimensional function space over the space-time slab Q_n (with $H_0^{1h}(Q_n) \subset H_0^1(Q)$, where $H_0^1(Q)$ denotes the Sobolev space of square-integrable functions and square integrable first derivatives and zero value on the boundary).

In weak form, the space-time formulation of equations (1, 2, 5 and 6) can be written as follows (taking care of the above dimensionless form for the Navier – Stokes equations):

Find $\mathbf{U}^h \in \left(S_{\mathbf{U}}^h\right)_n$ and $P^h \in \left(S_P^h\right)_n$, such that: $\forall \mathbf{W}^h \in \left(V_{\mathbf{U}}^h\right)_n$ and $\forall q^h \in \left(V_P^h\right)_n$

$$\begin{aligned}
&\int_{Q_n} \mathbf{W}^h \cdot \left(\frac{\partial \mathbf{U}^h}{\partial \tau} + \mathbf{U}^h \cdot \nabla \mathbf{U}^h \right) dQ + \int_{Q_n} \boldsymbol{\varepsilon}\left(\mathbf{W}^h\right) : \boldsymbol{\sigma}\left(P^h, \mathbf{U}^h\right) dQ \\
&+ \int_{Q_n} q^h \nabla \cdot \mathbf{U}^h \, dQ + Ra \Pr \int_{Q_n} \mathbf{W}^h \cdot \left(\theta^h\right) \mathbf{e_g} \, dQ \\
&+ \Pr Ha^2 \int_{Q_n} \mathbf{W}^h \cdot \left(\nabla \Phi^h - \mathbf{U}^h \times \mathbf{e_B} \right) \times \mathbf{e_B} \, dQ \\
&+ \sum_{e=1}^{(n_{el})_n} \int_{Q_n^e} \tau_{stab} \left[\begin{array}{l} \left(\frac{\partial \mathbf{W}^h}{\partial \tau} + \mathbf{U}^h \cdot \nabla \mathbf{w}^h \right) - \nabla \cdot \boldsymbol{\sigma}\left(q^h, \mathbf{W}^h\right) \\ + \Pr Ra \theta^h \mathbf{e_g} + \Pr Ha^2 \left(\nabla \Phi^h - \mathbf{U}^h \times \mathbf{e_B} \right) \times \mathbf{e_B} \end{array} \right] \cdot \\
&\qquad \cdot \left[\begin{array}{l} \left(\frac{\partial \mathbf{U}^h}{\partial t} + \mathbf{U}^h \cdot \nabla \mathbf{U}^h \right) - \nabla \cdot \boldsymbol{\sigma}\left(P^h, \mathbf{U}^h\right) \\ + \Pr Ra \theta^h \mathbf{e_g} + \Pr Ha^2 \left(\nabla \Phi^h - \mathbf{U}^h \times \mathbf{e_B} \right) \times \mathbf{e_B} \end{array} \right] dQ = 0 \quad (7)
\end{aligned}$$

We note that if we were using a standard finite element formulation, rather than this space-time technique, the Galerkin formulation of equations (1, 2, 5 and 6) would have consisted of the first five integrals. The remaining series of integrals are the least-squares terms added to the Galerkin variational formulation to assure the numerical stability of the computations. The coefficient τ_{stab} determines the weight of such added terms.

2.2.3 Stabilized Streamline Upwind Petrov-Galerkin (SUPG) formulation for Convection-Diffusion Equation

For the heat transfer equation we also adopt the SUPG stabilization in work by Ed Akin and Tezduyar (2004); using suitably-defined finite-dimensional trial solution and test function spaces

$$\left(S_\theta^h\right)_n =$$
$$\left\{\theta^h \mid \theta^h \in \left[H^{1h}(Q_n)\right]^{n_{sd}},\ \theta^h = \theta_D \text{ on } (P_n)_g,\ \mathbf{n}\cdot\nabla\theta^h = h \text{ on } (P_n)_h\right\} \left(V_\theta^h\right)_n =$$
$$\left\{w^h \mid w^h \in \left[H^{1h}(Q_n)\right]^{n_{sd}},\ w^h = 0 \text{ on } (P_n)\right\}$$

The stabilized finite element formulation of the previously written energy equation with boundary and initial conditions can be written as follows: find $\theta^h \in S_\theta^h$ such that $\forall w^h \in V_\theta^h$:

$$\int_{Q_n} w^h \left(\frac{\partial\theta^h}{\partial\tau} + \mathbf{U}^h\cdot\nabla\theta^h\right) dQ + \int_{Q_n} \nabla w^h \cdot \mathrm{Pr}\nabla\theta^h dQ - \int_{P_h} w^h h\, dP$$
$$+ \sum_{e=1}^{(nel)_n} \int_{Q_n^e} \tau_{SUPG}\mathbf{U}^h\cdot\nabla w^h \left(\frac{\partial\theta^h}{\partial\tau} + \mathbf{U}^h\cdot\nabla\theta^h - \mathrm{Pr}\nabla^2\theta^h\right) dQ$$

Here τ_{SUPG} is the SUPG stabilization parameter.

2.2.4 Standard Galerkin FEM for Electrical Potential Equation

The classical Galerkin formulation is adopted for the electrical potential equation.

After spatial discretization of the weak forms of the governing equations, a system of nonlinear ordinary differential equations is obtained for the solution of the velocity $\mathbf{U}$, the pressure P, the temperature θ, and the electric potential field Φ in the domain.

For time integration an implicit method known as "Backward Differentiation Formulas (BDF)" is used. The matrix system obtained was numerically solved using the geometric multigrid with SOR (Successive Over-Relaxation) as smoother. The equations are solved by a two level fixed V-cycle procedure starting with the coarsest grid level and progressing to the finer one (for details see Hackbusch (1985)).

3 Results and Discussion

3.1 Model Validation

The simulation results obtained here are compared with those of Bennacer, El Ganaoui and Leonardi (2006) and Sheu, Rani, Tan and Tsai (2007), who investigated a similar geometry for different Ra numbers. The results are presented in terms of the averaged Nusselt number (Nu_{av}) values at the bottom and the top surfaces, and tabulated in Tab. 1. The results are in good agreement (the maximum relative error is found to be less than 4%).

3.2 Steady Symmetric Flow (at Low Ra)

The only control parameter in this part is the Rayleigh number *Ra*, which is a non-dimensional measure of ΔT. For small (*Ra*), the buoyancy force arising from the heated surfaces (bottom and two lateral ones) is balanced by the viscosity of the fluid, and thus heat travels from the heated section towards the top surface mainly by conduction.

Convective and conductive heat fluxes, along lines across the centre of the cavity in the *Z*and *Y*-directions, are presented in Fig. 2. It is shown that for moderate values of *Ra* (e.g. *Ra = 100*) the heat transfer is mainly conductive with a weak contribution from convection (Figs. 2a), due to weakly convective flow resulted for these values. For relatively height values of *Ra* (*Ra* = 2800) convective transport is more important (Fig. 3b). Convection is due to the fluid motion induced by the applied temperature gradient on the laterally heated surfaces. This is because the fluid is heated from the side then the gravity is orthogonal to the density gradient, and thus convection arises at any value of the *Ra* number.

The resulting flow structure for this range of *Ra* consists of two counter-rotating main cells inside the cavity, as shown in Figs. 3 (a, b) by the velocity vectors in the vertical mid-plane (Y=0.5). The hot fluid rises up along the heating lateral walls and moves down in the lateral mid-plane (Z=0.5). This motion brings cold fluid from the top to the bottom wall through the centre of the cavity. The resulting flow for this *Ra* range exhibits a weak spiral flow structure, similar to a 2D flow structure in a deep cavity see Bennacer, El Ganaoui and Leonardi (2006). In the current geometry, the flow field is expected to be symmetric with respect to the plane Z=0.5 and Y=0.5 (corresponding to symmetrical planes of the present cavity) (see the velocity component in the X-direction U plotted in the plane X=0.5 in Fig. 4a) also it exhibits symmetry with respect to the diagonal plane joining the points with coordinates (0, 0, 0), (1, 0, 0), (1, 1, 1) (Fig. 4b).

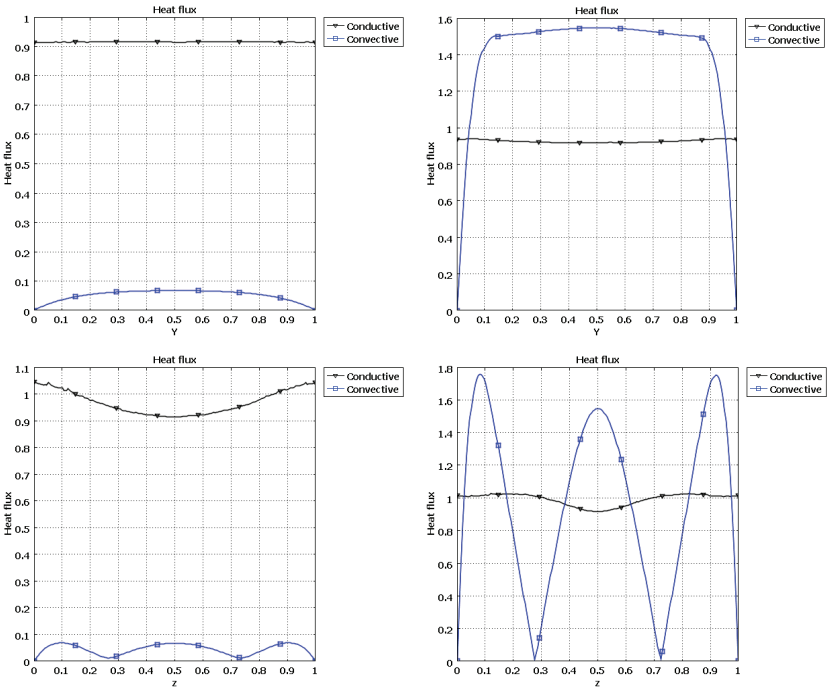

Figure 2: Heat fluxes along the lines across the centre of the cavity in the Y, Z-directions, respectively, for Ra=100 and Ra=2800

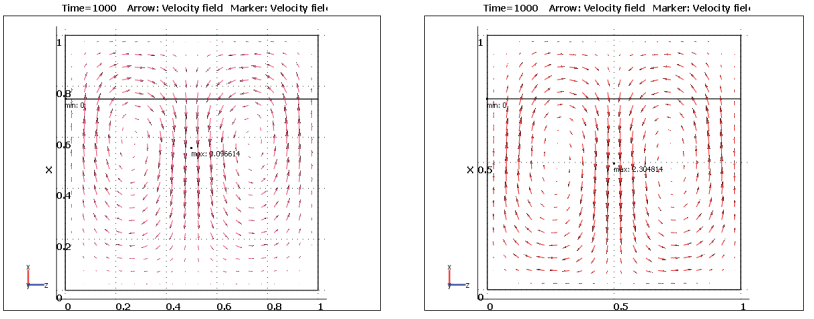

Figure 3: Velocity vectors in the vertical mid-plane (Y=0.5) for different Ra values, (steady state), symmetry with respect (Z=0.5) for Ra=100 and Ra=2800

Table 1: Comparaison of results.

Ra		1000	2000	3000	4000
Top	Present	-2.1593	-2.1647	-2.1717	-2.1783
	Bennacer	-2.12	-2.13	-2.14	-2.15
	Sheu	-2.1077	-2.1134	-2.1308	–
Bottom	Present	0.2769	0.30092	0.32316	0.3352
	Bennacer	0.279	0.304	0.310	0.337
	Sheu	0.28061	0.30438	0.31148	–
Approx. Value of Ra_{cr} & Method	Present	$\approx$ 2810,Stabilized FEM with tetrahedral non-uniform mesh consists of 62872 elements			
	Bennacer	<3000, Finite volume with non-uniform mesh with 82 x 82 x 82			
	Sheu	3040, Finite volume with uniform mesh with 41 x 41 x 41			

3.3 Central-Steady- Breaking and Transition

At the Ra value around ($\approx$ 2810) a central symmetry breaking appears. A transition from steady state symmetric flow to non-symmetric flow is observed. Indeed, when Ra reaches its critical value the initially observed central symmetry of the steady flow disappears, and the flow begins to become non-symmetric. This symmetry breaking is a known feature of the present kind of the cavity geometry with rigid boundaries. We think that, this symmetry breaking and the transition from steady symmetric flow to non-symmetric flow results in due to the lateral temperature gradient. Transition to steady or time dependency is a function of the geometry and the type of boundary conditions used. The strong dependence of the critical parameters on the geometry and on the boundary conditions of the cavity is reported in Gelfgat, Bar-Yoseph and Yarin (1999). The flow remains symmetric with respect to the plane of symmetry Z=0.5 (Fig. 5). A break in symmetry occurred vertically (Y-direction) and in the diagonal plane joining points (0, 0, 0), (1, 0, 0), (1, 1, 1) (Fig. 5b). The symmetry vanishes with respect to the vertical mid-plane (Y=0.5) (Fig. 5c).

The break in symmetry in the thermal field may also be illustrated, as shown in Fig. 6a, by the conductive and the convective heat fluxes distributions along line across the centre of the cavity in Y-direction. It is observed that we have break in symmetry with respect to the mid-plane (Y=0.5). However, the symmetry remains with respect to the mid-plane (Z=0.5), as seen in Fig. 6b, by the conductive and

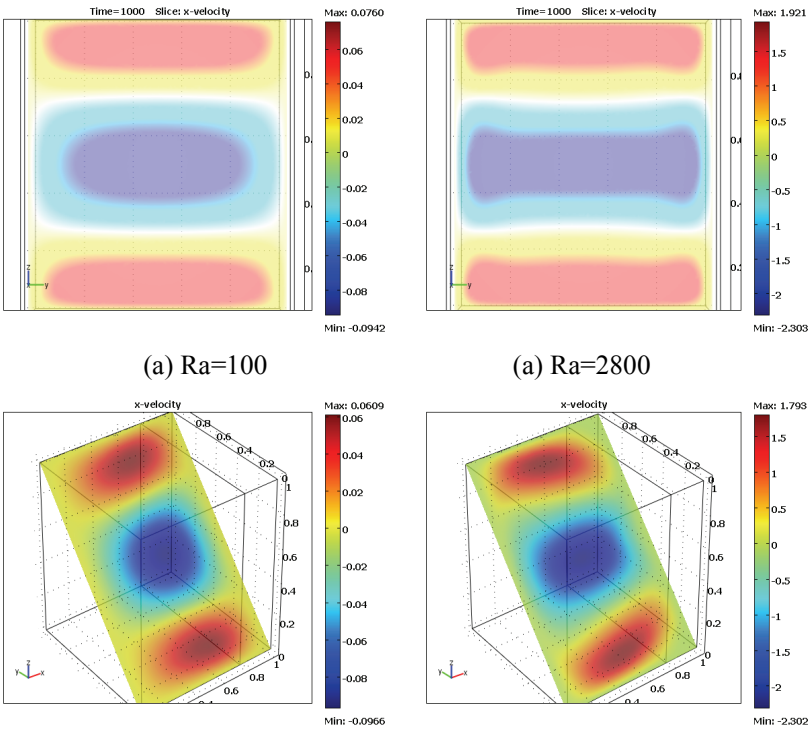

(a) Ra=100 (a) Ra=2800

(b) Ra=100 (b) Ra=2800

Figure 4: Steady velocity component in the X-direction on plane (X=0.5) and on the diagonal plane joining points with coordinates (0,0,0), (1,0,0), (1,1,1), for different moderate Ra: (a) Symmetry with respect the vertical mid-plane (Y=0.5) as well as the lateral mid-plane (Z=0.5); (b) Symmetry in this diagonal plane.

convective heat fluxes along line across the centre of the cavity in Z-direction.

3.4 Application of an external horizontal magnetic field

The flow under the effect an applied magnetic field is more stable than that of the first case, (Ha = 0), because of the stabilizing effects of the magnetic body force acting on the points of the fluid. For example, for the case where Ha = 2, steady symmetric flows are obtained with Ra less than to 3×10^3. Transition from steady symmetric to steady asymmetric flow develops for this case (Ha = 2) when Ra is around ($\approx 3 \times 10^3$). At this Ra value a break in symmetry occurs in the mid-plane (Y = 0.5) and in the diagonal plane. Qualitatively, steady and time

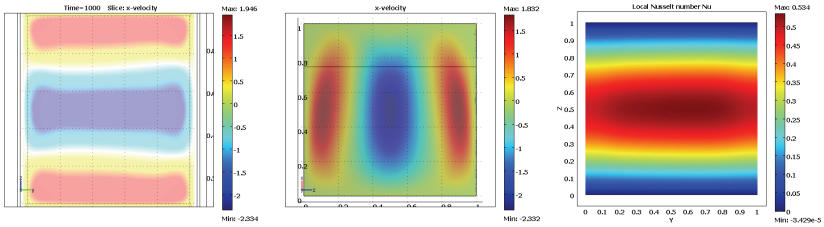

Figure 5: The distribution of U velocity in the plane X=0.5 and on the diagonal plane and the distribution of Nu at the bottom X=0, for Ra=2850. The symmetry remains with respect Z=0.5, symmetry vanishes in the plane Y=0.5 and the diagonal plane.

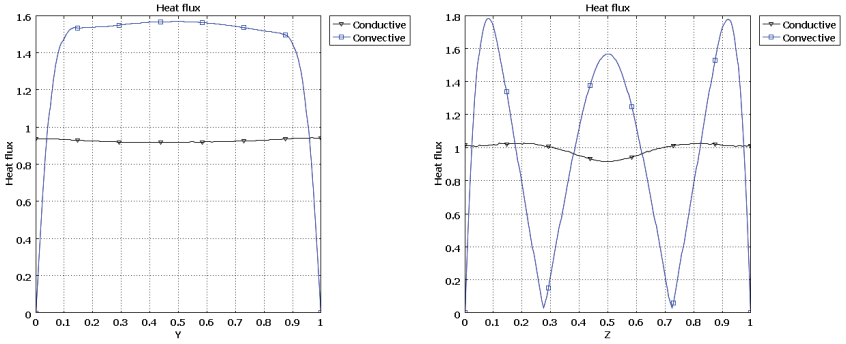

Figure 6: Symmetry breaking illustration by the distribution of heat fluxes along the line across the centre of the cavity in the Y-direction, for Ra=2850, (a) break in symmetry with respect the mid-plane (Y=0.5), (b) symmetry remains in the plane (Z=0.5)

dependent flow fields obtained for the present case (Ha = 2) are similar to steady and time dependent flow fields of the previous case (Ha = 0). For this case (Ha = 2), the computed maximal and minimal values of steady symmetric convective flow velocity components are weak with respect to those of the first case (Ha = 0) (Tab. 2).

Further increase in Ha leads to flows more stable and weak (Tab. 4 and Figs. 7). Examination of Tab. 4 and Figs. 7 reveals that for each Ra value the flow becomes weaker with increasing Ha. Thus, the magnetic field suppressing the flow field

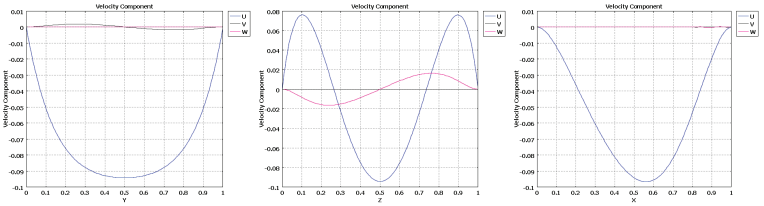

Ha = 0, Ra= 100

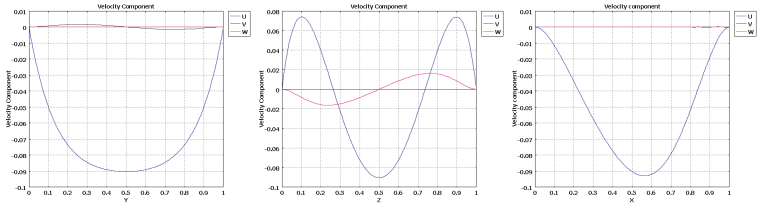

Ha=2, Ra=100

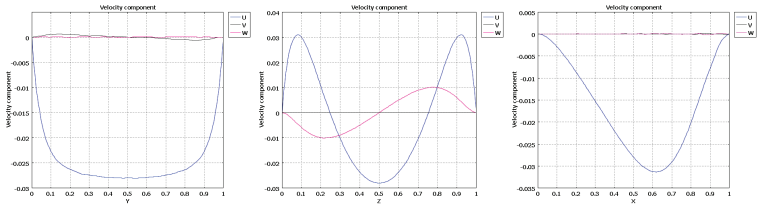

Ha=15, Ra=100

Figure 7: Damping effects of the applied magnetic field (at Ra = 100): (a) Line across the centre of the cavity in the Y-direction, (b) Line across the centre of the cavity in the Z-direction, and (c) Line across the centre of the cavity in the X-direction.

has a stabilizing effect, and retards the central-symmetry breaking bifurcation even for higher Ha values (see Tab. 4). Indeed, the applied magnetic field damps and makes uniform mainly the X-component velocity as it is seen in Figs. 7. The velocity component in the Z-direction was also found to be reduced. For example, the maximum averaged X- and Z- velocity component values (at Ha = 0) were reduced approximately by 3 and 2 times, respectively, at Ha = 15 (Fig. 7).

Table 2: Maximum and minimum steady dimensionless velocities in the cavity at Ra= 100 and at different Ha (from 0 to 50) and corresponding approximated critical values.

Ha	U		V		W		Approx.
	Max	Min	Max	Min	Max	Min	Ra_{cr}
0	0.082083	-0.096614	0.003344	-0.00331	0.055022	-0.055121	2.81×10^3
1	0.081573	-0.095659	0.003189	-0.003159	0.054679	-0.054779	2.9×10^3
2	0.080097	-0.092908	0.002844	-0.00292	0.053678	-0.053779	3×10^3
4	0.074747	-0.083455	0.002215	-0.002196	0.050035	-0.050143	3.4×10^3
6	0.067355	-0.071524	0.00179	-0.001823	0.045012	-0.045131	4.2×10^3
8	0.059606	-0.059773	0.001725	-0.001631	0.039627	-0.03973	5.3×10^3
10	0.052409	-0.049599	0.001911	-0.001752	0.034612	-0.03476	6.7×10^3
15	0.03788	-0.031366	0.001889	-0.001714	0.024217	-0.024175	1.4×10^4
20	0.028139	-0.020972	0.001611	-0.001473	0.017497	-0.017518	2.5×10^4
30	0.017728	-0.011098	0.001123	-0.001016	0.010054	-0.010149	7.45×10^4
40	0.012093	-0.006838	0.000895	-0.000736	0.006496	-0.00652	1.6×10^5
50	0.008909	-0.004642	0.000673	-0.000572	0.004569	-0.004511	2.5×10^5

4 Conclusion

In this work three-dimensional simulations were presented for a simplified vertical Bridgman configuration heated from below. An increase in the flow strength may lead to non-symmetrical flow structures or unsteadiness for lower controlling parameters (Ra number). The effect of the Ra number on the flow structure and heat transfer distribution is shown.

The simulations results are compared with those of the literature. The break in symmetry occurred at relatively lower Ra numbers in comparison with the 2-D models. The present analysis also illustrates the limitation of 2-D simulations in identifying such transitions. The flow becomes three-dimensional at relative low Ra numbers, and the preliminary results illustrate the effect of the depth of the cavity on the mean flow and indicate the existence of a wavelength in the third direction.

The application of an external magnetic field presents itself as a promising tool for damping and stabilizing the flow structures.

References

Achoubir, K.; Bennacer, R.; Cheddadi, A.; El Ganaoui, M.; and Semma E.; (2008): Numerical Study of Thermosolutal Convection in Enclosures Used for Directional Solidification (Bridgman Cavity), *FDMP: Fluid Dynamics and Material Processing*, Vol. 4, No. 3, pp. 199-210

Armour, N.; Yildiz, M.; Yildiz, E.; Dost, S. (2008): Liquid Phase Diffusion

Growth of SiGe under Magnetic Fields, *ECS Transactions*, vol. 16(10), pp. 135-146.

Bennacer, R.; El Ganaoui, M.; Leonardi, E. (2006): Symmetry breaking of melt flow typically encountered in a Bridgman configuration heated from below, *Applied Mathematical Modelling,* vol. 30, pp. 1249–1261.

Bucchignani E. (2009): An Implicit Unsteady Finite Volume Formulation for Natural Convection in a Square Cavity, *FDMP: Fluid Dynamics and Material Processing*, Vol. 5, No. 1, pp. 37-60

Dennis, B.H.; Dulikravich, G.S. (2002): Magnetic field suppression of melt flow in crystal growth, *International Journal of Heat and Fluid Flow*, vol.23, pp. 269–277

Dost, S.; Lent, B. (2007): Single Crystal Growth of Semiconductors from Metallic Solutions, Elsevier, Amsterdam, The Netherlands,

Dost, S.; Okano Y. (Editors), (2007): Crystal Growth Under Applied Fields," Research Signpost, 37/661 (2), Trivandrum-695 023, Kerala, India.

Ed Akin, J., Tezduyar, T.E., (2004): Calculation of the advective limit of the SUPG stabilization parameter for linear and higher-order elements, *Comput. Methods Appl. Mech. Engrg.,* vol. 193, pp. 1909–1922.

El Ganaoui, M.; Bontoux, P. (1998): An homogenisation method for solid–liquid phase change during directional solidification, Numerical and Experimental Methods in Heat Transfer, *ASME, HTD*, vol. 361(5), pp. 453–469.

Gelfgat, A.Y. (1999): Different Modes of Rayleigh–Bénard Instability in Two- and Three-Dimensional Rectangular Enclosures, *Journal of Computational Physics,* vol. 156, pp. 300–324.

Gelfgat, A.Y.; Bar-Yoseph, P.Z.; Solan, A. (2001): Effect of axial magnetic field on three-dimensional instability of natural convection in a vertical Bridgman growth configuration, *J. Cryst. Growth*, 230, pp. 63-72.

Gelfgat, A.Y.; Bar-Yoseph, P.Z.; Yarin, A.l. (1999): Non-symmetric convection flows in laterally heated rectangular cavities, *IJCFD*, vol.11, pp. 261–273.

Gelfgat, A.Y.; Bar-Yoseph, P.Z.; Yarin, A.l. (1999): Stability of multiple steady states of convection in laterally heated cavities, *J. Fluid Mech.,* vol. 388, pp. 315–334.

Hackbusch, W. (1985): Multi-grid Methods and Applications, Springer-Verlag, Berlin.

Hof, B.; Juel, A.; Mullin, T. (2003): Magnetohydrodynamic damping of convective flows in molten gallium, *J. of Fluid Mechanics*, vol. 482, pp.163-179.

Hurle, D.T.J. (1966): Temperature oscillations in molten metals and their relationship to growth striate in melt-grown crystals. *Phil. Mag.* vol.13, pp. 305-310.

Hurle, D.T.J.; Jakeman E.; Johnson, C.P. (1974): Convective Temperature Oscillations in Molten Gallium, *J. Fluid Mech.*, vol. 64(3), pp. 565-576.

Impey, M.D.; Riley, D.S.; Wheeler, A.A.; Winters, K.H. (1991): Bifurcation analysis of solutal convection during directional solidification, *Phys. Fluids*, vol. A3 (4), , pp. 535–550.

Kakimoto, K. and Liu, L., (2006), Flow instability of silicon melt in magnetic fields, *FDMP: Fluid Dynamics and Material Processing*, Vol. 2, No.3, pp.167-174.

Kumar, V.; Dost, S.; Durst, F. (2007): Numerical Modeling of Crystal Growth under Strong Magnetic Fields: An Application to the Traveling Heater Method," *Appl. Math. Modelling*, vol. 31, pp. 589-605.

Liu, Y. C.; Dost, S.; Sheibani, H. (2004): A Three Dimensional Simulation for the Transport Structures in Liquid Phase Electroepitaxy under Applied Magnetic Field," *Int. J. Transport Phenomena*, vol. 6, pp. 51-62.

Liu, Y.C.; Dost, S.; Lent, B.; Redden, R.F. (2003): A Three-Dimensional Numerical Simulation Model for the Growth of CdTe Single Crystals by the Traveling Heater Method under Magnetic Field, *J. Crystal Growth*, vol. 254, pp. 285-297.

Müller, G.; Ostrogorsky, A. (1994): Convection in melt growth. In Handbook of Crystal Growth. (ed. D. T. J. Hurle), North-Holland, Amsterdam, vol. 2, pp. 711-781.

Okada K.; Ozoe, H. (1992): Experimental heat transfer rates of natural convection of molten gallium suppressed under an external magnetric field in either the X, Y, or Z direction," *J. Heat Transfer* , vol. 114 (1), pp. 107-114.

Piazza, I. Di; Ciofalo, M. (2002): MHD free convection in a liquid-metal filled cubic enclosure: I. Differential heating *Inter. J. of Heat and Mass Transfer*, vol. 45, pp. 1477–1492.

Prud'homme, R. and El Ganaoui, M., (2007), Solid/Liquid Phase Change: Recent Studies and Models, *FDMP: Fluid Dynamics and Material Processing*, Vol. 3, No. 2, pp. 161-172

Sahu, S.; Muralidhar, K. and Panigrahi, P.K., (2007), Interface Deformation and Convective Transport in Horizontal Differentially Heated Air-Oil Layers, *FDMP: Fluid Dynamics and Material Processing*, Vol. 3, No. 3, pp. 265-286.

Sheibani, H.; Dost, S.; Sakai, S.; Lent, B. (2003): Growth Of Bulk Single Crystals Under Applied Magnetic Field By Liquid Phase Electroepitaxy," *J. Crystal Growth*, vol. 258(3-4), pp. 283-295.

Sheu, T.W.H.; Rani, H.P.; Tan, T.-C.; Tsai, S.F. (2007): Multiple states, topology and bifurcations of natural convection in a cubical cavity, *Computers & Fluids,* vol. 37, no. 8, pp. 1011-1028.

Sohail, M. and Saghir, M.Z., (2006): Three-Dimensional Modeling of the Effects of Misalignment on the Growth of Ge1-xSix by The Traveling Solvent Method, *FDMP: Fluid Dynamics and Material Processing*, Vol. 2, No.2, pp.127-140.

Tezduyar, T.E. (1992): Stabilized finite element formulations for incompressible flow computations, *Adv. Appl. Mech.,* vol. 28, pp. 1-44.

Tezduyar, T.E.; Mittal, S.; Ray, S. E.; Shih, R. (1992): Incompressible flow computations with stabilized bilinear and linear equal-order-interpolation velocity-pressure elements, *Comput. Meth. Appl. Mech. Eng.,* vol. 95, pp. 221-242.

Touihri, R.; Ben Hadid, H.; Henry, D. (1999): On the onset of convective instabilities in cylindrical cavities heated from below: I- Pure thermal case, *Phys. Fluids*, vol. 11, pp. 2078.

Yildiz, E.; Dost, S. (2007): The Combined Effect of Rotating and Static Magnetic Fields in Liquid Phase Diffusion Growth of SiGe, *J. Crystal Growth*, vol. 303(1), pp. 279-283.